Nematic twist–bend phase in an external field

Grzegorz Pająk[a,b,1], **Lech Longa**[a], **and Agnieszka Chrzanowska**[b]

[a]Marian Smoluchowski Institute of Physics, Department of Statistical Physics, Jagiellonian University, Łojasiewicza 11, 30-348 Kraków, Poland; [b]Faculty of Physics, Mathematics and Computer Science, Tadeusz Kościuszko Cracow University of Technology, Podchorążych 1, 30-084 Kraków, Poland

This manuscript was compiled on December 15, 2017

The response of the nematic twist–bend (N_{TB}) phase to an applied field can provide important insight into structure of this liquid and may bring us closer to understanding mechanisms generating mirror symmetry breaking in a fluid of achiral molecules. Here we investigate theoretically how an external uniform field can affect structural properties and stability of N_{TB}. Assuming that the driving force responsible for the formation of this phase is packing entropy we show, within Landau–de Gennes theory, that N_{TB} can undergo a rich sequence of structural changes with field. For the systems with positive anisotropy of permittivity we first observe a decrease of the tilt angle of N_{TB} until it transforms through a field–induced phase transition to the ordinary prolate uniaxial nematic phase (N). Then, at very high fields this nematic phase develops polarization perpendicular to the field. For systems with negative anisotropy of permittivity the results reveal new modulated structures. Even an infinitesimally small field transforms N_{TB} to its elliptical counterpart ($N_{\mathrm{TB}e}$), where the circular base of the cone of the main director becomes elliptic. With stronger fields the ellipse degenerates to a line giving rise to a nonchiral periodic structure, the nematic splay–bend (N_{SB}), where the two nematic directors are restricted to a plane. The three structures, N_{TB}, $N_{\mathrm{TB}e}$ and N_{SB}, with a modulated polar order are globally nonpolar. But further increase of the field induces phase transitions into globally polar structures with nonvanishing polarization along the field's direction. We found two such structures, one of which is a polar and chiral modification of N_{SB}, where splay and bend deformations are accompanied by weak twist deformations ($N^{*}_{\mathrm{SB}_p}$). Further increase of the field unwinds this structure into a polar nematic (N_p) of polarization parallel to the field.

twist–bend nematic | splay–bend nematic | chirality | polarity

The twist–bend nematic (N_{TB}) phase, recently discovered in liquid–crystalline chemically achiral dimers (1–7), bent–core mesogens (8, 9), and their hybrids (10), is one of the most amazing example of spontaneous chiral symmetry breaking in soft matter physics. It occurs in the liquid state without any long–range positional order, but the average local molecular long axis, $\hat{\mathbf{n}}$, known as the director, follows a nanoscale–pitch heliconical winding. Thus the structure belongs to the family of nematic phases and is the fifth nematic phase recognized (5), in addition to uniaxial and biaxial nematics for nonchiral liquid crystalline materials and cholesteric and blue phases for chiral liquid crystals (11). In 2001 Dozov (12), following earlier analysis of Meyer (13, 14), predicted theoretically this structure using Frank model of elastic deformations in nematics by assuming that the bend elastic constant can change sign. With this assumption $\hat{\mathbf{n}}$ can form 1D modulated structures where simultaneously twist and bend or splay and bend elastic constants are nonzero. The second of the structures, known as the nematic splay–bend (N_{SB}), is nonchiral and exhibits periodic splay and bend modulations of the director, taking place within one plane. The observation of this phase is still not confirmed experimentally, but it can be stabilized in constant pressure Monte–Carlo simulations of thin layers composed of hard bent–core molecules (15).

The first possibility is recognized as the chiral N_{TB} phase with the director, $\hat{\mathbf{n}}(\mathbf{r}) \equiv \hat{\mathbf{n}}(z)$, attaining oblique helicoidal structure in precessing on the side of a right circular cone, Fig. 1. More specifically

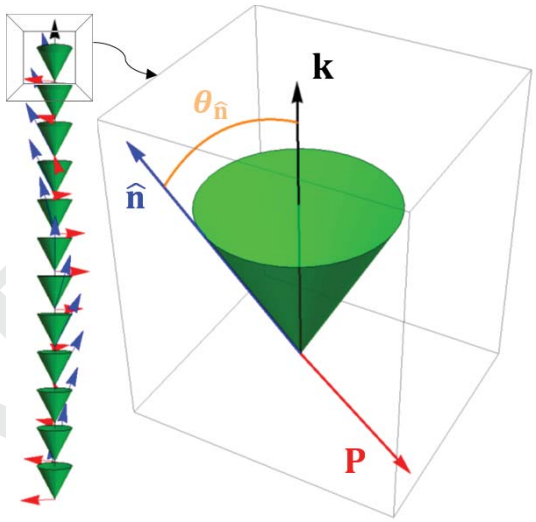

Fig. 1. (Color online) Schematic representation of the nematic twist–bend structure. Right circular cone of angle $\theta_{\hat{\mathbf{n}}}$ shows the tilt between the director $\hat{\mathbf{n}}$ and the helical symmetry axis, parallel to the wave vector, $\mathbf{k}$. Red arrows represent $\mathbf{P}$, where $\mathbf{P} \parallel \mathbf{k} \times \hat{\mathbf{n}}$; black arrow is the direction of $\mathbf{k}$.

Significance Statement

The twist–bend nematic liquid crystalline phase is the fifth nematic structure recognized in nature (5), and its stabilization is explained by assuming a coupling between polar and nematic orderings. It exhibits macroscopically chiral heliconical orientational order on the ten–nanometer scale and represents a unique example of spontaneous chiral symmetry breaking for system of *achiral* molecules. Understanding of how an external field affects the stability of this phase can shed further light on the origin of this induced twist and is of relevance to potential applications. Within mesoscopic Landau–de Gennes theory we find that for compounds with positive anisotropy the helix unwinds to a polar nematic, however negative material anisotropy gives rise to a rich sequence of new nematic phases obtained via mechanism of flattening the conical spiral.

All authors contributed in research, analysis of data and preparing the manuscript.

The authors declare no conflict of interest.

[1]To whom correspondence should be addressed. E-mail: grzegorz@th.if.uj.edu.pl and postal address[b].

$$\hat{\mathbf{n}}(z) = [\cos(\phi_{\hat{\mathbf{n}}})\sin(\theta_{\hat{\mathbf{n}}}), \sin(\phi_{\hat{\mathbf{n}}})\sin(\theta_{\hat{\mathbf{n}}}), \cos(\theta_{\hat{\mathbf{n}}})], \quad [1]$$

where $\theta_{\hat{\mathbf{n}}}$ is the conical angle (angle between $\hat{\mathbf{n}}$ and $\mathbf{k}$) and $\phi_{\hat{\mathbf{n}}} = \pm kz = \pm\frac{2\pi}{p}z$ with wave vector $\mathbf{k} = k\hat{\mathbf{z}}$ taken to be parallel to the $\hat{\mathbf{z}}$–axis of laboratory system of frame; here p is the pitch. The Dozov's scenario for the formation of $N_{\rm TB}$ has strong experimental support for anomalously small, but positive values of the bend elastic constant have been reported in the nematic phase as the transition to $N_{\rm TB}$ was approached (4, 16). A Landau–de Gennes mesoscopic theory, where the director is replaced by a symmetric and traceless tensor order parameter field, $\mathbf{Q}$, accounts for a fine structure of the modulated phases and shows limitations of the director's description (17, 18).

The $N_{\rm TB}$ phase observed has a number of remarkable features. It looks uniform everywhere in space like cholesterics, with a temperature–dependent conical angle, $\theta_{\hat{\mathbf{n}}}$, ranging approximately between 9° and 30° (4, 19, 20). But, while the cholesteric phase with its conical angle equal to a right angle ($\theta_{\hat{\mathbf{n}}} = \pi/2$), can homogeneously fill the space with twist the analogous arrangement for $N_{\rm TB}$ ($0 < \theta_{\hat{\mathbf{n}}} < \pi/2$) requires both bend and twist deformations to be present. X-ray diffraction experiments, sensitive to positional (3, 5) or orientational (21, 22) orderings reveal no long–range positional order of molecular centers of mass ($N_{\rm TB}$ indeed remains a fully 3D liquid), but a 1D periodic order of molecular orientations. The helicoidal pitch length in the $N_{\rm TB}$ is about 10 nm, *i.e.* on the order of a few molecular lengths, which is about two orders of magnitude smaller than that typically found in cholesteric and blue phases (11). The $N_{\rm TB}$ phase is usually stabilized as a result of a first–order phase transition from the uniaxial nematic phase, but very recently a direct transition between $N_{\rm TB}$ and the isotropic phase has also been found (23, 24). Lack of molecular intrinsic chirality implies that coexisting domains of opposite handedness are formed and, consequently, the emergence of $N_{\rm TB}$ is related to a fundamentally new phenomenon, namely, *the spontaneous chiral symmetry breaking.*

While phenomenologically the spontaneous distortion of the $N_{\rm TB}$ and $N_{\rm SB}$ phases can effectively be explained as originating from the negative bend elasticity (12) the question of what microscopic/mesoscopic mechanism can be responsible for chiral symmetry breaking, especially the selforganization into $N_{\rm TB}$, is still open and remains to be understood and explored. The issue has been addressed at the theoretical level in a series of papers (18, 25–33). Analysis shows that the molecules whose structure is sufficiently bent is a necessary requirement for the stabilization of $N_{\rm TB}$, probably as a results of entropic, excluded volume interactions (25, 28). The molecules not only selforganize into a helical structure, but also propagate long–range polar order of vanishing global polarization, transverse to the helical axis. For steric interactions the polarity is a consequence of ordering of molecular bent cores (27, 28, 32, 33) and the other molecular interactions, like between electrostatic dipoles, are probably less relevant for thermal stability of this phase. These conclusions seem in line with recent experimental observations (34–36).

A mesoscopic–level explanation of how molecular polarity of bent–core molecules can generate modulated polar phases and, hence, effectively lower the bend elastic constant has been proposed to be due to the flexoelectric couplings, where derivatives of the the alignment tensor (or of the director field), induce a net polarization (17, 18, 26, 29, 37). The minimal coupling model, which is able to account for $N_{\rm TB}$, is the Landau–de Gennes (LdeG) type of free energy expansion in the alignment tensor $\mathbf{Q}(\mathbf{r})$ and the polarization field $\mathbf{P}(\mathbf{r})$, and their derivatives (17, 18, 38). It can be decomposed as

$$F \equiv F[\mathbf{Q},\mathbf{P}] = \frac{1}{V}\int_V (f_Q + f_P + f_{QP})\,\mathrm{d}^3\mathbf{r}, \quad [2]$$

where the free energy densities, f_X, are constructed out of the fields $\{X\}$. By taking suitable units and assuming deformations to appear only in a quadratic part of the free energy, the general form of f_X up to fourth order in X for nonchiral liquid crystals is (17)

$$\begin{aligned} f_Q &= \frac{1}{4}\left[t_Q\,\mathrm{Tr}(\mathbf{Q}^2) + (\nabla\otimes\mathbf{Q})\cdot(\nabla\otimes\mathbf{Q})\right. \\ &+ \left.\rho(\nabla\cdot\mathbf{Q})\cdot(\nabla\cdot\mathbf{Q})\right] - \sqrt{6}\,B\,\mathrm{Tr}(\mathbf{Q}^3) + \mathrm{Tr}(\mathbf{Q}^2)^2, \quad [3] \end{aligned}$$

$$\begin{aligned} f_P &= \frac{1}{4}\left[t_P\,\mathbf{P}^2 + (\nabla\otimes\mathbf{P})\cdot(\nabla\otimes\mathbf{P}) + a_c(\nabla\cdot\mathbf{P})^2\right] \\ &+ (\mathbf{P}^2)^2, \quad [4] \end{aligned}$$

$$f_{QP} = -\frac{1}{4}e_P\mathbf{P}\cdot(\nabla\cdot\mathbf{Q}) - \lambda P_\alpha Q_{\alpha\beta}P_\beta, \quad [5]$$

where t_Q and $t_P > 0$ are the reduced temperatures associated with $\mathbf{Q}$ and $\mathbf{P}$ fields, respectively; ρ is the relative elastic constant; a_c is the strength of longitudinal contribution from the steric polarization (18); e_P is the strength of flexopolarization. For thermodynamic stability of this free energy expansion it is also mandatory that $\rho > -\frac{3}{2}$ and $1+a_c > 0$. When the flexopolarization coupling becomes strong enough ($\rho - \frac{e_P^2}{4t_P} \leq -\frac{3}{2}$) (18), the uniform nematic phase can no longer be stable and a modulated polar phase is formed. In addition to $N_{\rm TB}$ and $N_{\rm SB}$ the theory (2) predicts the existence of further two 1D modulated nonchiral, polar nematic phases with transverse and longitudinal polarization being modulated along just one direction for one star of wave vector approximation (18). But it is important to observe that the flexopolarization term alone ($e_P \neq 0$) is not sufficient to bring about spontaneous chiral symmetry breaking. It needs to be accompanied, at least, by the nonvanishing λ–coupling ($\lambda \neq 0$) in F. The nonvanishing λ is also needed for a proper explanation of the fluctuation modes in $N_{\rm TB}$, as suggested by recent light scattering experiments (39).

Alternative mesoscopic scenarios pertaining to the stability of $N_{\rm TB}$, like these involving couplings between the alignment tensor and higher rank (octupolar) order parameters have also been proposed (40–46). This indicates that the theoretical studies of mechanism(s) responsible for observed spontaneous chiral symmetry breaking are still in their initial stage and further research is needed to provide understanding of stability of $N_{\rm TB}$. One promising direction, which we would like to follow here, is a systematic analysis of how properties of $N_{\rm TB}$ can change in the presence of external stimuli, such as electric or magnetic fields, surface anchoring, photo–chemically driven trans–cis isomerization *etc.* Such analysis can also be important in seeking for future practical applications of this new phase.

In case of modulated nematics their response to an external field can become highly nontrivial (11, 47). In cholesterics, for example, it is possible to unwind the orientational spiral

through an intermediate heliconical structure (48, 49), both for bulk sample (50) and in confined geometry (51, 52). A more comprehensible, field–induced modification of cholesterics involves reorientation of helical axis (11), or changing the pitch (53). Similar effects can be expected for $N_{\rm TB}$, although recent magnetic field experiments (54, 55) show only depletion of the $N-N_{TB}$ transition temperature, without a noticeable distortion of the structure. So far, theoretical attempts to characterize the interaction of $N_{\rm TB}$ with field have been made on the basis of the Frank elastic theory (56–58).

A purpose of this paper is to study, in a systematic way, a response of the bulk $N_{\rm TB}$ phase to the external fields (electric, magnetic) within the frame of the LdeG free energy, Eqs. (2-5). As $N_{\rm TB}$ is expected for nonchiral bent–shaped molecules, with and without electric dipoles, we assume that stability of this phase is driven primarily by excluded–volume, entropic interactions (28). We consider the LdeG free energy, Eq. 2, supplemented by the dielectric (diamagnetic) term, F_E, ($F\rightarrow F+F_E$), where

$$F_E=-\Delta\epsilon\frac{1}{V}\int_V E_\alpha Q_{\alpha\beta}(\mathbf{r})E_\beta \mathrm{d}^3\mathbf{r}, \qquad [6]$$

and where $\Delta\epsilon$ is the dielectric (diamagnetic) anisotropy in the director reference frame. We think that the dielectric (diamagnetic) term should dominate, at least for sufficiently strong fields and disregard a possible direct interaction between the dipole moments and the field. We explore the absolute stability of the $N_{\rm TB}$ phase for the model (2-6) by limiting to a family of all nematic structures, periodic at most in one spatial direction (hereafter referred to as ODMNS (18)). Starting with the $N_{\rm TB}$ phase, which is stable within the ODMNS family for vanishing field, we identify free energy minimizers for nonzero field (59). A full account of the electric field response, with terms quadratic and linear in field, will be presented elsewhere.

All possible ODMNS structures can be parameterized with the aid of plane waves expansion of $\mathbf{Q}(\mathbf{r})$ and $\mathbf{P}(\mathbf{r})$ (17, 18): $\mathbf{Q}(\mathbf{r})=\sum_n\sum_{m=-2}^{2}Q_m(n)\exp(\mathrm{i}\,nk\,\hat{\mathbf{z}}\cdot\mathbf{r})\,\mathbf{e}^{[2]}_{m,\hat{\mathbf{z}}}$, $\mathbf{P}(\mathbf{r})=\sum_n\sum_{m=-1}^{1}P_m(n)\exp(\mathrm{i}\,nk\,\hat{\mathbf{z}}\cdot\mathbf{r})\,\mathbf{e}^{[1]}_{m,\hat{\mathbf{z}}}$, where $nk\hat{\mathbf{z}}=\mathbf{k}$ are the wave-vectors ($n=0,\pm1,...$); $Q_m(n)$ and $P_m(n)$ are the unknown amplitudes found from the minimization of the free energy expansion, and $\mathbf{e}^{[L]}_{m,\hat{\mathbf{z}}}$, $m=0,\pm1,\pm L$ are the spin $L=1,2$ spherical tensors represented in a laboratory coordinate system with quantization axis along $\hat{\mathbf{z}}$-direction. The selection of k, $Q_m(n)$, and $P_m(n)$ is fixed by minimization of F, supplemented by the bifurcation analysis (37, 60, 61). Note that only $n=0$ terms couple to a uniform external field in (6), giving

$$F_E=-\Delta\epsilon E^2\left\{\sin^2(\theta)\left[x_{20}\cos(2\phi)-y_{20}\sin(2\phi)\right]+\sin(2\theta)\right.$$
$$\left.\left[y_{10}\sin(\phi)-x_{10}\cos(\phi)\right]+x_{00}\left[3\cos(2\theta)+1\right]/(2\sqrt{6})\right\}, \qquad [7]$$

where $\mathbf{E}=E[\cos(\phi)\sin(\theta),\sin(\phi)\sin(\theta),\cos(\theta)]$ is the external field expressed in the laboratory system of frame and where $\mathfrak{Re}Q_m(n)=x_{mn}$ and $\mathfrak{Im}Q_m(n)=y_{mn}$. The relative orientation of $\mathbf{Q}$ and $\mathbf{E}$, parameterized by θ and ϕ, is found by minimization of F. The formulas (3-5) entering F are given in the expanded form in (37).

Our starting point is the identification of homogeneous structures of wave vector k that can be constructed out of $\mathbf{Q}$ and $\mathbf{P}$, among which should be the $N_{\rm TB}$ phase. The spatial homogeneity of a structure implies that $\forall z$ the tensors $\mathbf{Q}(z)$ and, say, $\mathbf{Q}(0)$ for $z=0$ are connected by a rotation. More specifically, $\mathbf{Q}(z)$ can be obtained from $\mathbf{Q}(0)$ by rotating through the angle kz about $\hat{\mathbf{z}}$: $\mathcal{R}_{\hat{z}}(\pm kz)\mathbf{Q}(0)=Q_\pm(z)$, where $\pm$ stands for right– and left–handed heliconical structure. Likewise, through the same rotation $\mathbf{P}(0)$ is transformed into $\mathbf{P}(z)$: $\mathcal{R}_{\hat{z}}(\pm kz)\mathbf{P}(0)=\mathbf{P}_\pm(z)$. The structures fulfilling the above conditions have a *unique* form given by the terms of $|n|\leq 2$ in the expansions of $\mathbf{Q}$ and $\mathbf{P}$, namely

$$\mathbf{Q}_\pm(z)=Q_0(0)\mathbf{e}^{[2]}_{0,\hat{\mathbf{z}}}+\sum_{m=1}^{2}\left[Q_{\pm m}(m)\mathbf{e}^{[2]}_{\pm m,\hat{\mathbf{z}}}e^{\pm imkz}+c.c\right], \qquad [8]$$

$$\mathbf{P}_\pm(z)=P_0(0)\mathbf{e}^{[1]}_{0,\hat{\mathbf{z}}}+\left[P_{\pm1}(1)\mathbf{e}^{[1]}_{\pm1,\hat{\mathbf{z}}}e^{\pm ikz}+c.c\right]. \qquad [9]$$

For example, the explicit formulas for $\mathbf{Q}_+$ and $\mathbf{P}_+$ read

$$\mathbf{Q}(z)\equiv\mathbf{Q}_+(z) = \begin{bmatrix} \cos(2kz+\phi_2)r_2-\frac{x_{00}}{\sqrt{6}} & -\sin(2kz+\phi_2)r_2 & -\cos(kz+\phi_1)r_1 \\ -\sin(2kz+\phi_2)r_2 & -\cos(2kz+\phi_2)r_2-\frac{x_{00}}{\sqrt{6}} & \sin(kz+\phi_1)r_1 \\ -\cos(kz+\phi_1)r_1 & \sin(kz+\phi_1)r_1 & \sqrt{\frac{2}{3}}x_{00} \end{bmatrix}, \qquad [10]$$

$$\mathbf{P}(z)\equiv\mathbf{P}_+(z) = \begin{bmatrix} -\sqrt{2}p_1\cos(kz+\phi_p) \\ \sqrt{2}p_1\sin(kz+\phi_p) \\ v_{00} \end{bmatrix}. \qquad [11]$$

Here $r_i\cos(\phi_i)=x_{ii}$, $r_i\sin(\phi_i)=y_{ii}$ ($r_i\geq0$), $p_1\cos(\phi_p)=v_{11}$, $p_1\sin(\phi_p)=z_{11}$ ($p_1\geq0$), where $v_{ij}=\mathfrak{Re}P_i(j)$, $z_{ij}=\mathfrak{Im}P_i(j)$ and, as previously, $x_{ij}=\mathfrak{Re}Q_i(j)$ and $y_{ij}=\mathfrak{Im}Q_i(j)$. Note that one of the three phases ϕ_i, ($i=1,2,p$) is the Goldstone mode and can be eliminated, which expresses the freedom of choosing the origin of the laboratory system of frame. In what follow we set $\phi_1=0$. Hence, a family of all homogeneous (polar) helical nematic mesophases, structurally linked with the uniaxial nematic phase (N), can be parameterized unambiguously using at most eight parameters (including k vector). The x_{00} terms in Eq. (10) represents the reference N phase with the director along $\hat{\mathbf{z}}$. As the systems we study are nonchiral, the spontaneous chiral symmetry breaking means that domains representing opposite chiralities have the same free energy: $F[\mathbf{Q}_+,\mathbf{P}_+]=F[\mathbf{Q}_-,\mathbf{P}_-]$ and that they are formed with the same probability (ambidextrous chirality).

Setting $r_1=0$ in Eq. (10) gives the cholesteric phase of the conical angle $\theta_{\hat{\mathbf{n}}}=\pi$, Eq. (1), while the simplest of the $N_{\rm TB}$ phases is obtained by neglecting terms with $m=2$ ($r_2=0$)

in (10). In this simplified case the conical angle is given by

$$\cos(\theta_{\hat{\mathbf{n}}}) = \frac{\sqrt{3\chi^2+8}+\sqrt{3}\chi}{\sqrt{2}\sqrt{3\chi^2+\sqrt{9\chi^2+24}\chi+8}}, \qquad [12]$$

where $\chi = x_{00}/r_1$. Note that $0 \leq \theta_{\hat{\mathbf{n}}} \leq \pi/4$ for prolate uniaxial nematic background ($x_{00} \geq 0$), while the oblate case ($x_{00} \leq 0$) yields $\pi/2 \geq \theta_{\hat{\mathbf{n}}} \geq \pi/4$. The general case of N_{TB} with $r_2 \neq 0$ allows for a fine control of biaxiality and of the conical angle. For example, the biaxiality of $N_{\rm TB}$, measured by the normalized parameter w (62)

$$-1 \leq w(\mathbf{Q}) = \sqrt{6}\, Tr(\mathbf{Q}^3)/\left[Tr(\mathbf{Q}^2)\right]^{\frac{3}{2}} \leq 1\,, \qquad [13]$$

is given by

$$w = \frac{\chi\left(-6\tau^2+\chi^2+3\right)+3\sqrt{6}\,\tau\cos(\phi_2)}{(2\tau^2+\chi^2+2)^{3/2}}. \qquad [14]$$

Here $\tau = r_2/r_1$ and $w = 1$ ($w = -1$) for local uniaxial prolate (oblate) order. The states of $|w| < 1$ are biaxial with $w = 0$ corresponding to maximally biaxial order. Note that w, Eq. (14), is k–independent, expressing the fact that z–dependence of $\mathbf{Q}$, Eq. (10), is generated by a rotation. This means that $N_{\rm TB}$ is biaxial and in the limit of $k \to 0$ we get the fourth of homogeneous nematic structures accounted for by (10), namely the biaxial nematic.

Each of the structures identified so far can be polar, Eq. (11). For $k \neq 0$ the polarization can acquire the long–range periodic component in the $x-y$ plane ($p_1 \neq 0$), which is perpendicular to $\hat{\mathbf{z}}$ and/or global macroscopic polarization ($v_{00} \neq 0$), parallel to $\hat{\mathbf{z}}$. Interestingly, the $N_{\rm TB}$ phase given by Eqs (10,11) with $v_{00} = 0$, can be the global minimizer within the ODMNS class. The sufficient condition for the free energy parameters can be derived using the bifurcation analysis (37) with uniaxial nematic ($x_{00} \neq 0$) as a reference state. It reads

$$\frac{-2\sqrt{6}t_P}{\sqrt{9B^2-8t_Q}+3B} < \lambda < \frac{\sqrt{\frac{3}{2}}\left(e_P^2-4(\rho+2)t_P\right)}{(\rho+2)\left(\sqrt{9B^2-8t_Q}+3B\right)}, \qquad [15]$$

which is valid when the following additional constrains are fulfilled: $e_P \neq 0$, $t_Q < B^2$, $\rho > -\frac{3}{2}$ and $t_P > 0$.

In seeking for a globally stable structure among ODMNS we need to take into account both homogeneous and inhomogeneous trial states given by the plane waves expansion of $\mathbf{Q}$ and $\mathbf{P}$. The complexity of the ODMNS minimization depends on the number of amplitudes used in this expansion, which is controlled by the maximal value n_{max} of $|n|$ in the set $\{k, Q_m(n), P_m(n),\ n = 0, \pm1, ..., \pm n_{max}\}$. As it turns out the $n_{max} = 1$ approximation with 25 *real*, variational parameters is not sufficient to qualitatively reproduce structural changes as experienced by $N_{\rm TB}$ due to an applied external field. In order to obtain credible results the following strategy has proved to work. In the first step we perform the free energy minimization with $n_{max} = 2$. Then, the identified structures serve in the next step as initial states in seeking for the improved free energy minimum, where relaxation method for 1D periodic structures is being used for the bulk sample. A short summary of this typical method is given in Supporting Information (SI).

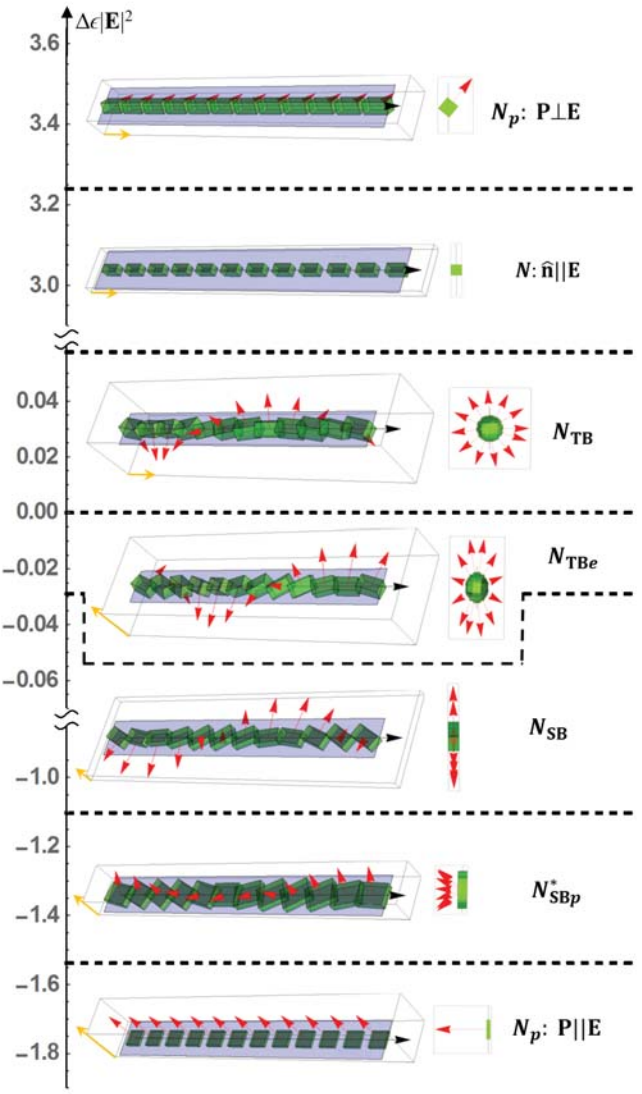

Fig. 2. (Color online) Sketch of $N_{\rm TB}$ modifications under the external field. Dashed lines correspond to the strength of external field coupling that leads to a phase transformation; yellow arrows are directions of $\mathbf{E}$ in each of the structures. Red arrows represent $\mathbf{P}$ and black arrow is the direction of $\mathbf{k}$. Lengths of cuboid edges are proportional to the eigenvalues of $\mathbf{Q}+c\mathbf{I}$, where $\mathbf{I}$ is the unit matrix and c is a constant, such that the isotropic state is represented by a cube. Every phase is presented in a perspective with its top view added.

Results of numerical analysis are illustrated for the case when $\rho = 1$, $a_c = 2$, $e_P = -4$, $B = 1/\sqrt{6}$, $\lambda = -1/2$, $t_Q = 1/10$ and $t_P = 8/10$ where without external field the heliconical structure gives minimum among ODMNS, isotropic, uniaxial and biaxial nematics. Depending on the strength of the field and the sign of the material anisotropy, both controlled by the single model parameter $\Delta\epsilon E^2$ in Eq. (6), the $N_{\rm TB}$ structure evolves as shown in Fig. (2). For the case of positive material anisotropy ($\Delta\epsilon E^2 > 0$) the minimum is realized for $\mathbf{E}||\hat{\mathbf{k}}$, while for negative anisotropy ($\Delta\epsilon E^2 < 0$) the minimum occurs when $\mathbf{E}\perp\hat{\mathbf{k}}$. Furthermore, in the positive anisotropy case the $N_{\rm TB}$ phase unwinds to the uniaxial nematic with the director parallel to the external field. Further increase of the field results in stabilization of a polar nematic (N_p), where secondary director is parallel to the polarization

vector, both being perpendicular to the external field. The case of negative anisotropy modifies instantly the modulation of the main director in the $N_{\rm TB}$ phase, which is now precessing on the right elliptic cone around $\hat{\mathbf{k}}$. We denote this new structure as $N_{\rm TBe}$. Stronger fields ($\mathbf{E}\perp\hat{\mathbf{k}}$) make the elliptic cone base narrower and finally $N_{\rm SB}$ is stabilized, where the cone becomes degenerated to a line and $\mathbf{P}$ lies in the plane of splay–bend modulations. With larger fields in–plane modulations diminish and $\mathbf{P}$ acquires the off-plane uniform component along the field. This is a new chiral structure denoted $N^*_{\rm SBp}$. For even stronger fields this phase transforms to polar nematic with polarization parallel to the field.

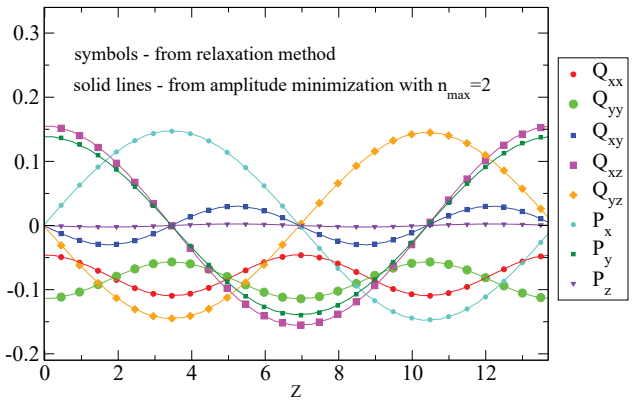

Fig. 3. (Color online) $\mathbf{Q}$ and $\mathbf{P}$ fields obtained for $N_{\rm TB}$ from the relaxation method (symbols) and from the free energy minimization with respect to the Fourier amplitudes for $n_{max}=2$ (lines) for $\Delta\epsilon E^2=0.0025$.

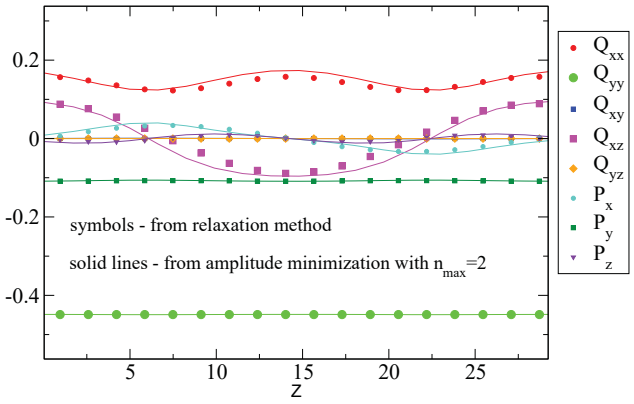

Fig. 4. (Color online) $\mathbf{Q}$ and $\mathbf{P}$ fields obtained for $N^*_{\rm SBp}$ from the relaxation method (symbols) and from the free energy minimization with respect to the Fourier amplitudes for $n_{max}=2$ (lines) for $\Delta\epsilon E^2=-1.3225$.

Quantitatively phases are described by the amplitudes $Q_m(n)$ and $P_m(n)$, or equivalently by their real and imaginary parts, which we denoted: $x_{ij}=\mathfrak{Re}Q_i(j)$, $y_{ij}=\mathfrak{Im}Q_i(j)$, $v_{ij}=\mathfrak{Re}P_i(j)$, $z_{ij}=\mathfrak{Im}P_i(j)$. Additionally each structure is characterized by the wave vector k. For stable ODMNS with $n_{max}=2$ the sets of nonzero parameters are: $\{y_{11},y_{22},x_{00},x_{11},x_{22},z_{11},v_{11}\}$ for $N_{\rm TB}$; as in $N_{\rm TB}$ and $\{y_{-22},y_{-11},y_{02},x_{-22},x_{-11},x_{02},x_{20},z_{-11},z_{02},v_{-11},v_{02}\}$ for $N_{\rm TBe}$; as in $N_{\rm TBe}$, provided that the following constrains are fulfilled $\{|y_{-22}|=|y_{22}|,|y_{-11}|=|y_{11}|,|x_{-22}|=|x_{22}|,|x_{-11}|=|x_{11}|,|z_{-11}|=|z_{11}|,|v_{-11}|=|v_{11}|\}$ for $N_{\rm SB}$; and as in $N_{\rm SB}$ in union with $\{|y_{-21}|=|y_{-12}|,|y_{12}|=|y_{21}|,|x_{-21}|=|x_{-12}|,|x_{12}|=|x_{21}|,|z_{-12}|=|z_{12}|,z_{10},|v_{-12}|=|v_{12}|\}$ for $N^*_{\rm SBp}$. A typical outcome of standard relaxation procedure, see (SI), for stable structures and how it compares with the amplitude minimization for $n_{max}=2$ is illustrated in Figs (3-9). Note that both the $n_{max}=2$ amplitude minimization and the relaxation results agree quantitatively, indicating that the approximation of $n_{max}=2$ is sufficient to obtain the basic features of the phases studied. Taking $n_{max}=1$ leads to qualitatively inconsistent results.

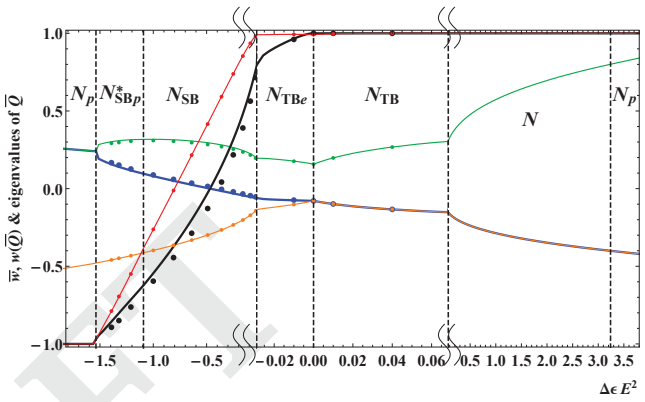

Fig. 5. (Color online) Various observables averaged over one period from the relaxation method (points) and from the free energy minimization with respect to the Fourier amplitudes for $n_{max}=2$ (lines). Eigenvalues of $\overline{Q}$ are given in green (along wave vector), orange (for negative anionotropy it is along the direction of external field) and blue. Biaxiality parameter, given by Eq. (13), is plotted in red for $\overline{w}$ and in black for $w(\overline{Q})$.

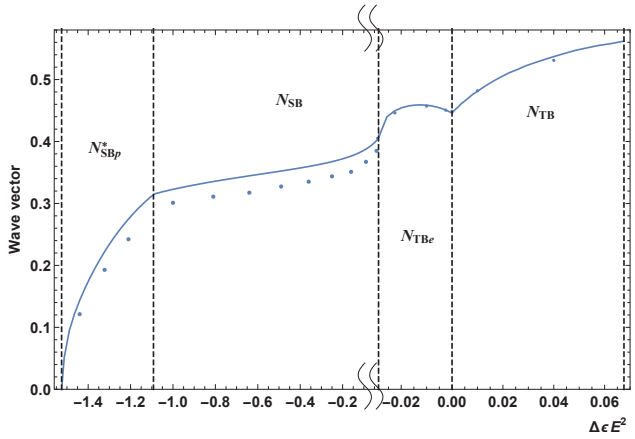

Fig. 6. (Color online) Wave vector as a function of external field for ODMNS presented in Fig. (2). As previously points are from relaxation method and line is outcome of the free energy minimization with respect to the Fourier amplitudes for $n_{max}=2$.

In order to give an insight into fine structure of stable phases we plot characteristic observables for each of them in Figs (5-9). Firstly, we present the behavior of eigenvalues for $\boldsymbol{Q}(z)$ averaged over one period ($\overline{\boldsymbol{Q}}$), Fig. (5), which is what can effectively be measured in experiments. Please note

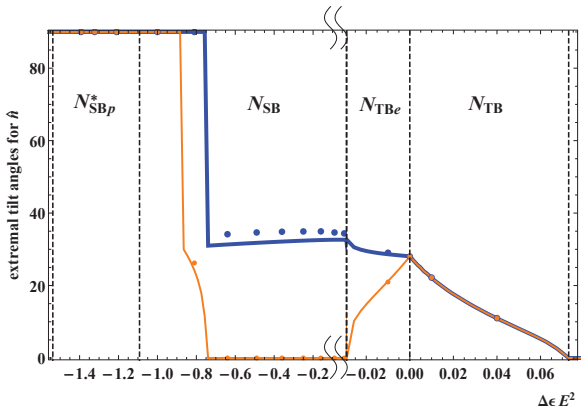

Fig. 7. (Color online) Minimal (orange) and maximal (blue) values of angle between $\mathbf{k}$ and $\hat{\mathbf{n}}$. As previously points are from relaxation method and lines are outcomes of the free energy minimization with respect to the Fourier amplitudes for $n_{max} = 2$.

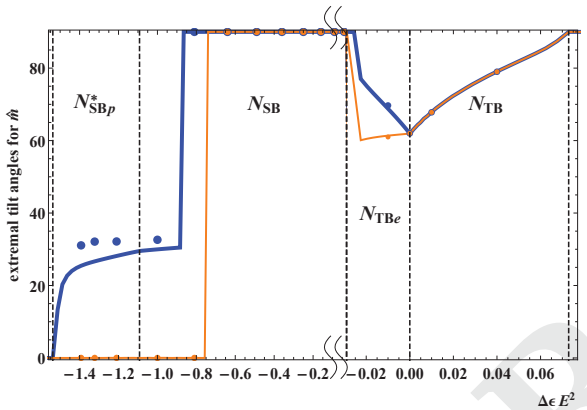

Fig. 8. (Color online) Minimal (orange) and maximal (blue) values of angle between $\mathbf{k}$ and $\hat{\mathbf{m}}$. As previously points are from relaxation method and lines are outcomes of the free energy minimization with respect to the Fourier amplitudes for $n_{max} = 2$.

that homogenous nematics and $N_{\rm TB}$ (averaged over one period) are uniaxial, as two eigenvalues of $\overline{\boldsymbol{Q}}$ coincide, and all other ODMNS are biaxial. Degree of biaxiality can be quantified by the relative differences between the eigenvalues, or with the help of the w parameter, Eq. (13). In Fig. (5) we present $w(\overline{\boldsymbol{Q}})$ in black, and $\overline{w}$ in red, and one sees that $N_{\rm TB}$ and $N_{{\rm TB}e}$ are weakly biaxial, as $\overline{w} < 1$, while $N_{\rm SB}$ is always biaxial passing the point of maximal biaxiality. Finally $N_{{\rm SB}p}$ is biaxial of oblate type and N_p is uniaxial oblate. Further important characteristic of ODMNS presented in Fig. (2) is the variation of the wave vector with field, which is shown in Fig. (6). Clearly, the wave vector vanishes in homogenous nematic phases. Note that the general effect of the field is to unwind the structures except for the initial behavior of $N_{{\rm TB}e}$, which is just opposite. Another variable which characterizes ODMNS is the conical angle. This tilt angle is measured between $\mathbf{k}$ and $\hat{\mathbf{n}}$, but could also be given *e.g.* between $\mathbf{k}$ and $\hat{\mathbf{m}}$. Being constant for N_{TB} it varies with z for all remaining ODMNS, as shown in Fig. (7), where we depict its minimal and maximal value with field. It is apparent that both semiaxes of ellipse are equal in $N_{\rm TB}$ (blue and orange lines in Fig. (7) coincide), but higher field makes the diameter of cone's basis smaller. In $N_{{\rm TB}e}$ blue and orange lines split providing the elliptic profile of the cone's basis. In the $N_{\rm SB}$ phase the minimal value of that angle is equal to zero and $\hat{\mathbf{m}}$, Fig. (8), is perpendicular to $\mathbf{k}$, which means that $\hat{\mathbf{n}}$ performs in–plane modulations between minimal and maximal values of $\theta_{\hat{\mathbf{n}}}$. Then, comparing Fig. (7) with Fig. (8) for the angle between $\mathbf{k}$ and $\hat{\mathbf{m}}$, gives insight into changing primary director from $\hat{\mathbf{n}}$ to $\hat{\mathbf{m}}$ as field increases for materials with negative anisotropy. This effect occurs when $\Delta\epsilon E^2 \cong -0.8$ and it is in fact caused by passing through a point of maximal biaxiality from prolate– to oblate–like structure, as shown in Fig. (5) for $\overline{w}$. Finally, in Fig. (9) we present the averages over one period for the length of polarization vector. Average of polarization modulus shows the average length of $\mathbf{P}$ for each structure, whereas modulus of averaged polarization reveals which of the phases posses the uniform component of $\mathbf{P}$.

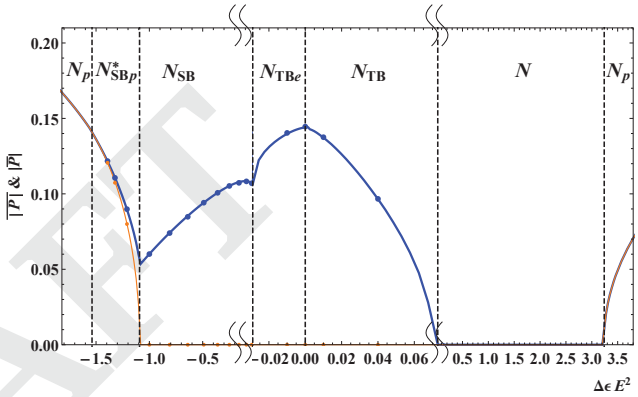

Fig. 9. (Color online) Averages over one period of $\overline{|P|}$ (blue) and $|\overline{P}|$ (orange). As previously points are from relaxation method and lines are outcomes free energy minimization with respect to the Fourier amplitudes for $n_{max} = 2$.

Summarizing, scientists have long sought to understand how chiral states can be generated in a liquid state from nonchiral matter. Now strong evidence is found that a new class of nematics called a nematic twist–bend provides such an example. This entropically induced state is realized because the underlying molecules have a specific shape. Here we presented possible transformations of the $N_{\rm TB}$ phase with an external field within the LdeG theory of flexopolarization. The outcomes of numerical minimization along with the full free energy relaxation method have been studied for few sets of model parameters, with one typical example being discussed in depth here.

For materials with positive anisotropy the unwinding of the helix to the uniaxial nematic structure is obtained, however here for sufficiently strong fields a polar nematic appears more stable. Compunds with negative anisotropy give rise to three different ODMNS with a wide range of the $N_{\rm SB}$ phase, so it is an apparent suggestion that this phase can be stabilized when applying external fields, and the experimental possibility for such an option has been presented before (63). So far the $N_{\rm SB}$ was expected as an intermediate state between neighboring domains of opposite chirality (19), which permits for smooth transition between adjacent right– and left–handed $N_{\rm TB}$ domains.

ACKNOWLEDGMENTS. This work was supported by the Grant

No. DEC-2013/11/B/ST3/04247 of the National Science Centre in Poland. GP acknowledges also support of Cracowian Consortium ‘,,Materia-Energia-Przyszłość” im. Mariana Smoluchowskiego’ within the KNOW grant.

1. Šepelj M, et al. (2007) Intercalated liquid-crystalline phases formed by symmetric dimers with an a,w-diiminoalkylene spacer. *J. Mater. Chem.* 17(12):1154–1165.
2. Panov VP, et al. (2010) Spontaneous periodic deformations in nonchiral planar-aligned bimesogens with a nematic-nematic transition and a negative elastic constant. *Phys. Rev. Lett.* 105(16):167801.
3. Cestari M, et al. (2011) Phase behavior and properties of the liquid-crystal dimer 1”,7”-bis(4-cyanobiphenyl-4’-yl) heptane: a twist-bend nematic liquid crystal. *Phys. Rev. E* 84(3 Pt 1):031704.
4. Borshch V, et al. (2013) Nematic twist-bend phase with nanoscale modulation of molecular orientation. *Nat. Commun.* 4:2635.
5. Chen D, et al. (2013) Chiral heliconical ground state of nanoscale pitch in a nematic liquid crystal of achiral molecular dimers. *Proc. Natl. Acad. Sci. USA* 110(40):15931–15936.
6. Paterson DA, et al. (2016) Understanding the twist-bend nematic phase: the characterisation of 1-(4-cyanobiphenyl-4’-yloxy)-6-(4-cyanobiphenyl-4’-yl)hexane (cb6ocb) and comparison with cb7cb. *Soft Matter* 12(32):6827–6840.
7. López DO, et al. (2016) Miscibility studies of two twist-bend nematic liquid crystal dimers with different average molecular curvatures. a comparison between experimental data and predictions of a landau mean-field theory for the ntb-n phase transition. *Phys. Chem. Chem. Phys.* 18(6):4394–4404.
8. Görtz V, Southern C, Roberts NW, Gleeson HF, Goodby JW (2009) Unusual properties of a bent-core liquid-crystalline fluid. *Soft Matter* 5(2):463–471.
9. Chen D, et al. (2014) Twist-bend heliconical chiral nematic liquid crystal phase of an achiral rigid bent-core mesogen. *Phys. Rev. E* 89(2):022506.
10. Wang Y, et al. (2015) Room temperature heliconical twist-bend nematic liquid crystal. *CrystEngComm* 17(14):2778–2782.
11. de Gennes PG, Prost J (1993) *The Physics of Liquid Crystals.* (Clarendon Press), 2 edition.
12. Dozov I (2001) On the spontaneous symmetry breaking in the mesophases of achiral banana-shaped molecules. *Europhys. Lett.* 56(2):247–253.
13. Meyer RB (1969) Piezoelectric effects in liquid crystals. *Phys. Rev. Lett.* 22(18):918–921.
14. Meyer RB (1976) *Proceedings of the Les Houches Summer School on Theoretical Physics, 1973, session No. XXV* eds. Balian R, Weil G. (Gordon and Breach), pp. 271–343.
15. Karbowniczek P, Cieśla M, Longa L, Chrzanowska A (2017) Structure formation in monolayers composed of hard bent-core molecules. *Liq. Cryst.* 44(1):254–272.
16. Adlem K, et al. (2013) Chemically induced twist-bend nematic liquid crystals, liquid crystal dimers, and negative elastic constants. *Phys. Rev. E* 88(2):022503.
17. Longa L, Trebin HR (1990) Spontaneous polarization in chiral biaxial liquid crystals. *Phys. Rev. A* 42(6):3453–3469.
18. Longa L, Pająk G (2016) Modulated nematic structures induced by chirality and steric polarization. *Phys. Rev. E* 93:040701.
19. Meyer C, Luckhurst GR, Dozov I (2015) The temperature dependence of the heliconical tilt angle in the twist-bend nematic phase of the odd dimer cb7cb. *J. Mater. Chem. C* 3(2):318–328.
20. Sreenilayam SP, Panov VP, Vij JK, Shanker G (2017) The ntb phase in an achiral asymmetrical bent-core liquid crystal terminated with symmetric alkyl chains. *Liq. Cryst.* 44(1):244–253.
21. Zhu C, et al. (2016) Resonant carbon k-edge soft x-ray scattering from lattice-free heliconical molecular ordering: Soft dilative elasticity of the twist-bend liquid crystal phase. *Phys. Rev. Lett.* 116(14):147803.
22. Stevenson WD, et al. (2017) Molecular organization in the twist-bend nematic phase by resonant x-ray scattering at the se k-edge and by saxs, waxs and gixrd. *Phys. Chem. Chem. Phys.* 19(21):13449–13454.
23. Archbold CT, Davis EJ, Mandle RJ, Cowling SJ, Goodby JW (2015) Chiral dopants and the twist-bend nematic phase–induction of novel mesomorphic behaviour in an apolar bimesogen. *Soft Matter* 11(38):7547–7557.
24. Dawood AA, et al. (2016) On the twist-bend nematic phase formed directly from the isotropic phase. *Liq. Cryst.* 43(1):2–12.
25. Memmer R (2002) Liquid crystal phases of achiral banana-shaped molecules: A computer simulation study. *Liq. Cryst.* 29(4):483–496.
26. Shamid SM, Dhakal S, Selinger JV (2013) Statistical mechanics of bend flexoelectricity and the twist-bend phase in bent-core liquid crystals. *Phys. Rev. E* 87(5):052503.
27. Greco C, Luckhurst GR, Ferrarini A (2014) Molecular geometry, twist-bend nematic phase and unconventional elasticity: a generalised maier-saupe theory. *Soft Matter* 10(46):9318–9323.
28. Greco C, Ferrarini A (2015) Entropy-driven chiral order in a system of achiral bent particles. *Phys. Rev. Lett.* 115(14):147801.
29. Osipov MA, Pająk G (2016) Effect of polar intermolecular interactions on the elastic constants of bent-core nematics and the origin of the twist-bend phase. *Eur. Phys. J. E* 39(4):45.
30. Vanakaras AG, Photinos DJ (2016) A molecular theory of nematic-nematic phase transitions in mesogenic dimers. *Soft Matter* 12(7):2208–2220.
31. Ferrarini A (2017) The twist-bend nematic phase: Molecular insights from a generalised maier–saupe theory. *Liq. Cryst.* 44(1):45–57.
32. Osipov MA, Pająk G (2017) Polar interactions between bent–core molecules as a stabilising factor for inhomogeneous nematic phases with spontaneous bend deformations. *Liq. Cryst.* 44(1):58–67.
33. Tomczyk W, Pająk G, Longa L (2016) Twist-bend nematic phases of bent-shaped biaxial molecules. *Soft Matter* 12(36):7445–7452.
34. Mandle RJ, et al. (2014) Synthesis and characterisation of an unsymmetrical, ether-linked, fluorinated bimesogen exhibiting a new polymorphism containing the n(tb) or ’twist-bend’ phase. *Phys. Chem. Chem. Phys* 16(15):6907–6915.
35. Ivsic T, Vinkovic M, Baumeister U, Mikleusevic A, Lesac A (2014) Retracted article: Milestone in the ntb phase investigation and beyond: direct insight into molecular self-assembly. *Soft Matter* 10(46):9334–9342.
36. Mandle RJ, et al. (2015) Apolar bimesogens and the incidence of the twist-bend nematic phase. *Chemistry - A European Journal* 21(22):8158–8167.
37. Longa L, Pająk G (2016). See Supplemental Material of [Phys. Rev. E **93**, 040701(R), 2016], which is avaiable at: http://journals.aps.org/pre/supplemental/10.1103/PhysRevE.93.040701/Supplemental_material.pdf.
38. Longa L, Monselesan D, Trebin HR (1987) An extension of the landau-ginzburg-de gennes theory for liquid crystals. *Liq. Cryst.* 2(6):769–796.
39. Parsouzi Z, et al. (2016) Fluctuation modes of a twist-bend nematic liquid crystal. *Phys. Rev. X* 6(2):021041.
40. Lubensky TC, Radzihovsky L (2002) Theory of bent-core liquid-crystal phases and phase transitions. *Phys. Rev. E* 66:031704.
41. Brand HR, Pleiner H, Cladis PE (2005) Tetrahedratic cross-couplings: Novel physics for banana liquid crystals. *Physica A* 351(2-4):189–197.
42. Longa L, Pająk G, Wydro T (2009) Chiral symmetry breaking in bent-core liquid crystals. *Phys. Rev. E* 79:040701.
43. Longa L, Pająk G (2011) Generalized dispersion model of orientationally ordered phases of bent–core liquid crystals. *Mol. Cryst. Liq. Cryst.* 541(1):152/[390]–158/[396].
44. Trojanowski K, Pająk G, Longa L, Wydro T (2012) Tetrahedratic mesophases, chiral order, and helical domains induced by quadrupolar and octupolar interactions. *Phys. Rev. E* 86:011704.
45. Longa L, Trojanowski K (2013) Ambidextrous chiral domains in nonchiral liquid-crystalline materials. *Acta Phys. Pol. B* 44(5):1201.
46. Trojanowski K, Cieśla M, Longa L (2017) Modulated nematic structures and chiral symmetry breaking in 2d. *Liq. Cryst.* 44(1):273–283.
47. Deuling HJ (1972) Deformation of nematic liquid crystals in an electric field. *Mol. Cryst. Liq. Cryst.* 19(2):123–131.
48. Xiang J, et al. (2015) Electrically tunable selective reflection of light from ultraviolet to visible and infrared by heliconical cholesterics. *Adv. Mater.* 27(19):3014–3018.
49. Salili SM, et al. (2016) Magnetically tunable selective reflection of light by heliconical cholesterics. *Phys. Rev. E* 94(4):042705.
50. Meyer RB (1968) Effects of electric and magnetic fields on the structure of cholesteric liquid crystals. *Applied Physics Letters* 12(9):281.
51. Scarfone AM, Lelidis I, Barbero G (2011) Cholesteric-nematic transition induced by a magnetic field in the strong-anchoring model. *Phys. Rev. E* 84:021708.
52. Zakhlevnykh AN, Shavkunov VS (2016) Magnetic-field-induced stepwise director reorientation and untwisting of a planar cholesteric structure with finite anchoring energy. *Phys. Rev. E* 94(4):042708.
53. Yang DK, Wu ST (2001) *Reflective liquid crystal displays*, Wiley SID series in display technology. (Wiley, Chichester Eng.).
54. Challa PK, et al. (2014) Twist-bend nematic liquid crystals in high magnetic fields. *Phys. Rev. E* 89(6):060501.
55. Salili SM, et al. (2016) Anomalous increase in nematic-isotropic transition temperature in dimer molecules induced by a magnetic field. *Phys. Rev. Lett.* 116(21):217801.
56. Meyer C (2016) Nematic twist-bend phase under external constraints. *Liq. Cryst.* 43(13-15):2144–2162.
57. Zola RS, Barbero G, Lelidis I, Rosseto MP, Evangelista LR (2017) A continuum description for cholesteric and nematic twist-bend phases based on symmetry considerations. *Liq. Cryst.* 44(1):24–30.
58. Shiyanovskii SV, Simonário PS, Virga EG (2017). *Liq. Cryst.* 44(1):31–44.
59. Chrzanowska A, Longa L (2016). ’Twist-bend nematic phase in the presence of external fields’ presented in part at the *Twist–Bend Nematics and Beyond Conference* in Southampton (2016).
60. Longa L (1986) On the tricritical point of the nematic–smectic a phase transition in liquid crystals. *J. Chem. Phys.* 85(5):2974.
61. Longa L, Grzybowski P, Romano S, Virga E (2005) Minimal coupling model of the biaxial nematic phase. *Phys. Rev. E* 71:051714.
62. Allender D, Longa L (2008) Landau–de gennes theory of biaxial nematics reexamined. *Phys. Rev. E* 78(1):011704.
63. Meyer C, Blanc C, Luckhurst GR, Dozov I (2015). Oral presentation entilted ’Electric-field induced twist-bend to splay-bend nematic transition?’ delivered during the 13th European Conference on Liquid Crystals in Manchester (2015).